Preprint typeset in JHEP style - HYPER VERSION

FSU-HEP-040505
UH-511-1050-04

Two Photon Background and the Reach of a Linear Collider for Supersymmetry in WMAP Favored Coannihilation Regions

Howard Baer and Tadas Krupovnickas

Department of Physics, Florida State University
Tallahassee, FL 32306, USA
E-mail: baer@hep.fsu.edu, tadas@hep.fsu.edu

Xerxes Tata

Department of Physics, University of Hawaii
Honolulu, HI 96822, USA
E-mail: tata@phys.hawaii.edu

Abstract: A neutralino relic density in accord with WMAP measurements can be found in the minimal supergravity (mSUGRA) model in several regions of parameter space: the stau co-annihilation corridor at low m_0 and the hyperbolic branch/focus point (HB/FP) region at large m_0 at the edges of parameter space, and the bulk and Higgs boson funnel regions within. In the regions at the edge, the mass gap between the next-to-lightest SUSY particle (NLSP) and the lightest SUSY particle (LSP) becomes small, and backgrounds from $\gamma\gamma \to f\bar{f}$ (f is a SM fermion) become important for NLSP detection at an e^+e^- linear collider. We evaluate these backgrounds from bremsstrahlung and beamstrahlung photons, and demonstrate that these do not preclude the observability of the signal for the cases where either the stau or the chargino is the NLSP. We also delineate the additional portion of the stau coannihilation region, beyond what can be accessed via a search for selectrons and smuons, that can be probed by a search for di-tau-jet events plus missing energy. The reach of a LC for SUSY in the HB/FP region is shown for an updated value of $m_t \simeq 180$ GeV as recently measured by the $D\emptyset$ experiment.

Keywords: Supersymmetry Phenomenology, e+e- Experiments, Dark Matter, Supersymmetric Standard Model.

1. Introduction

Weak scale supersymmetry is a highly motivated extension of the Standard Model (SM)[1]. In models with gravity-mediated supersymmetry breaking and R-parity conservation, the lightest SUSY particle is usually the lightest neutralino $\widetilde{Z}_1$, which is absolutely stable and serves as a good candidate particle for cold dark matter (CDM) in the universe[2]. Indeed, the recent precision mapping of anisotropies in the cosmic microwave background radiation by the WMAP collaboration[3, 4] has allowed a determination of

$$\Omega_{CDM}h^2 = 0.1126^{+0.0161}_{-0.0181} \tag{1.1}$$

at the 2σ level, where $\Omega = \rho_{CDM}/\rho_c$ is the ratio of the cold dark matter density to the critical mass density of the universe, and h is the scaled Hubble constant. This DM is unlikely to all be massive black holes (at least in our galactic halo) [5], or ordinary baryons (in the form of brown dwarfs) since a baryonic density of this magnitude would lead to conflicts with both Big Bang nucleosynthesis and the density of baryons as determined from the acoustic peaks in the CMB spectrum.

The minimal supergravity model (mSUGRA) forms a convenient template for exploring the experimental consequences of gravity-mediated SUSY breaking models[6]. The mSUGRA model is characterized by four SUSY parameters together with a sign choice,

$$m_0,\ m_{1/2},\ A_0,\ \tan\beta \ \text{ and } sign(\mu). \tag{1.2}$$

Here m_0 is the common mass parameter for all scalar particles at $Q = M_{GUT}$, $m_{1/2}$ is the common gaugino mass at M_{GUT}, A_0 is the common trilinear soft term at M_{GUT}, $\tan\beta$ is the ratio of Higgs field vacuum expectation values at the scale M_Z, and finally the magnitude – but not the sign – of the superpotential μ term is determined by the requirement of radiative electroweak symmetry breaking (REWSB). In addition, the top quark mass m_t must be specified. While the PDG quotes a value $m_t = 174.3 \pm 5.1$ GeV[7], we note that the $D\emptyset$ experiment has recently determined a value $m_t = 180.1 \pm 5.1$ GeV by a re-analysis of Run 1 data[8].

Over the years, several groups have evaluated the relic density of neutralinos in the context of the mSUGRA model[9, 10]. This has been recently re-examined in light of the WMAP data[11]. A value of $\Omega_{\widetilde{Z}_1}h^2$ in accord with the WMAP determination can be found in four broad regions of model parameter space:[1]

- The bulk annihilation region occurs at low m_0 and low $m_{1/2}$ for all $\tan\beta$ values. In this region, neutralino annihilation in the early universe occurs dominantly via t-channel exchange of light sleptons.

- The stau co-annihilation region occurs at low m_0 where $m_{\tilde{\tau}_1} \simeq m_{\widetilde{Z}_1}$, and where $\tilde{\tau}_1 - \widetilde{Z}_1$ and $\tilde{\tau}_1 - \bar{\tilde{\tau}}_1$ annihilation in the early universe serve to reduce the neutralino relic density to sufficiently low values[10],

[1] We note that the CDM may consist of several components, so that WMAP observation should be interpreted as an upper bound $\Omega_{\widetilde{Z}_1}h^2 < 0.129$ on the neutralino relic density. If we make the additional assumption that relic neutralinos consititute all the CDM, more stringent constraints are possible.

- the hyperbolic branch/focus point region[12, 13, 14] (HB/FP) at large m_0 near the edge of parameter space where μ becomes small, and the $\widetilde{Z}_1$ has a significant higgsino component which facilitates a large annihilation rate[15, 16, 17]. The location of this region is very sensitive to the value of m_t [18].
- the A-annihilation funnel at large $\tan\beta$ where m_H and $m_A \simeq 2m_{\widetilde{Z}_1}$ and $\widetilde{Z}_1\widetilde{Z}_1 \to A,\ H \to f\bar{f}$ (f's are SM fermions) through the very broad A and H resonances[9].

The bulk annihilation region is now disfavored and possibly excluded because it gives rise to values of m_h in violation of LEP2 limits, and can give large deviations from $BF(b \to s\gamma)$ and $(g-2)_\mu$[19]. A portion of the bulk annihilation region may survive, but only where it overlaps with the stau co-annihilation region or the A annihilation funnel. Other regions of parameter space may also give a reasonable relic density, including the stop co-annihilation region (for very particular A_0 values)[20] and the h annihilation corridor, where $2m_{\widetilde{Z}_1} \simeq m_h$.

Once the dark matter allowed regions of mSUGRA parameter space are identified, it is useful to see what the implications of these regions are for collider experiments. The reach of the Fermilab Tevatron[18, 21] and CERN LHC[22] have recently been worked out for the DM allowed regions of parameter space. In addition, the reach of a linear e^+e^- collider has also been investigated for the DM allowed regions of the mSUGRA model[23].

In Ref. [23], it was found that a $\sqrt{s} = 500 - 1000$ GeV LC could probe the entire stau co-annihilation region for $\tan\beta \lesssim 10$ by searching for selectron and smuon pair events. For higher $\tan\beta$ values, the stau co-annihilation region increases in $m_{1/2}$, while the reach for dilepton pairs decreases. The decrease in dilepton reach occurs mainly because the large-reach region is subsumed by the unallowed region where the $\tilde{\tau}_1$ becomes the LSP (a $\tilde{\tau}_1$ LSP is not allowed in R-conserving models because it would lead to charged stable relics from the Big Bang, for which there are stringent search limits). Some additional reach may be gained in the stau co-annihilation region by searching for stau pair production events, although this possibility was not investigated in Ref. [23].

The reach of a LC for SUSY in the HB/FP region was also examined in Ref. [23]. It was found that in this region a chargino pair production signal could be seen above SM background essentially up to the kinematic limit for production of two charginos at the LC. Standard cuts for identifying $\ell + 2 - jet$ events allowed chargino detection in the low $m_{1/2}$ portion of the HB/FP region. In the high $m_{1/2}$ portion of the HB/FP region, the $\widetilde{W}_1 - \widetilde{Z}_1$ mas gap became so small that specialized cuts were needed to pick out the signal from the background. In addition to usual SM backgrounds from the production of heavy particles (W, Z, t), contributions to backgrounds from $e^+e^- \to f\bar{f}$ and $\gamma\gamma \to f\bar{f}$ ($f = b, c$) were also included. The two photon cross sections were evaluated using Pythia[24] for the bremsstrahlung photon distribution, while the beamstrahlung contribution was not included. It was found that in the HB/FP region, an e^+e^- LC with $\sqrt{s} = 500 - 1000$ GeV could have a reach for SUSY considerably beyond that of the LHC!

It is significant that a neutralino relic density in accord with WMAP analyses occurs along the boundary of parameter space for both the stau co-annihilation case and the HB/FP region. In both these cases, the next-to-lightest SUSY particle (NLSP) becomes nearly degenerate in mass with the LSP. Thus, although NLSPs may be produced at

large rates at colliders, $NLSP \to LSP$ decays may result in only a small visible energy release, potentially making their detection difficult. This is because $\gamma\gamma \to f\bar{f}$ production, where the photons may originate from bremsstrahlung off the initial state electrons, or via beamstrahlung constitute an important background to the signal. In the stau co-annihilation region, we do not expect the two photon background to be problematic for the search for selectron or smuon pairs. The reason is that the e^+e^- or $\mu^+\mu^-$ pair originating from $\gamma\gamma$ annihilation is expected to come out back-to-back in the transverse plane for the background, but not so for the SUSY signal. However, for stau pair production, the $\gamma\gamma \to \tau\bar{\tau}$ background can be important, since the tau lepton is unstable, and the visible tau decay products will in general not be back-to-back in the transverse plane, especially when the daughter taus are relatively soft.

One of the purposes of this paper is a careful examination of the two photon background, including both bremsstrahlung and beamstrahlung contributions[25]. We describe our treatment of the $\gamma\gamma \to f\bar{f}$ background , and its inclusion into Isajet v7.70[26] in Sec. 2. We note here that it is likely that far forward detector elements reaching as close as 25 mrad of the beam line will likely be implemented in a realistic detector. The main purpose of the forward detectors will be to veto $\gamma\gamma$ or γe events where the initial $e^{\pm}$ suffers a slight deflection into the instrumented regions. In this work, we operate under the assumption that the initial state $e^{\pm}$ are collinear with the beam. In this sense, our results may be regarded as conservative.

In Sec. 3, we examine extending the LC reach for SUSY in the stau co-annihilation region by searching for signals with two tau jets plus missing energy[27]. The additional reach gained beyond that from the di-electron or di-muon channel is in fact substantial, especially for large $\tan\beta$. In Sec. 4, we re-examine the reach for SUSY by a LC in the HB/FP region, including the $\gamma\gamma \to b\bar{b}$ and $c\bar{c}$ background to ℓ + 2-jet events originating from both bremsstrahlung and beamstrahlung processes. The added background from beamstrahlung is substantial, but can be eliminated by invoking an additional angular cut in addition to cuts already suggested in Ref. [23]. We present updated reach results for one value of $\tan\beta$ at a higher value of $m_t = 180$ GeV as suggested by a recent DØ analysis[8]. In Sec. 5 we present a summary and conclusions of our results.

2. Two photon backgrounds

Our goal in this section is to evaluate the $e^+e^- \to f\bar{f}$ background including contributions from bremsstrahlung and beamstrahlung, and including two photon annihilation processes. In this case, the $e^+e^- \to f\bar{f}$ cross section is given by

$$\sigma(e^+e^- \to f\bar{f}) = \int dx_1 dx_2 \left[f_{e/e}(x_1,Q^2) f_{e/e}(x_2,Q^2) \hat{\sigma}(e^+e^- \to f\bar{f}) \right.$$
$$\left. + \left(f^{brem}_{\gamma/e}(x_1,Q^2) + f^{beam}_{\gamma/e}(x_1) \right) \left(f^{brem}_{\gamma/e}(x_2,Q^2) + f^{beam}_{\gamma/e}(x_2) \right) \hat{\sigma}(\gamma\gamma \to f\bar{f}) \right]. \quad (2.1)$$

Here, $f_{e/e}(x,Q^2)$ is the parton distribution function (PDF) for finding an electron inside

the electron, and is given by the convolution

$$f_{e/e}(x,Q^2) = \int_x^1 dz f_e^{brem}(\frac{x}{z},Q^2) f_e^{beam}(z)/z, \tag{2.2}$$

where $f_e^{brem}(x,Q^2)$ is the bremsstrahlung parton distribution function of the electron, and $f_e^{beam}(x)$ is the beamstrahlung parton distribution function of the electron. We use the Fadin-Kuraev distribution function for bremstrahlung electrons[28], given by

$$f_{e/e}^{brem}(x,Q^2) = \frac{1}{2}\beta\,(1-x)^{\frac{\beta}{2}-1}\left(1+\frac{3}{8}\beta\right) - \frac{1}{4}\beta\,(1+x)\,, \tag{2.3}$$

where $\beta = \frac{2\alpha}{\pi}(\log\frac{Q^2}{m_e^2} - 1)$. For the beamstrahlung distribution function of electrons in the electron, we use the parametrization of Chen[29], which is implemented in terms of the beamstrahlung parameter Υ (which depends in various characteristics of the beam profile), beam length σ_z (given in mm), and the beam energy E_e. For $f_{\gamma/e}^{brem}(x,Q^2)$, the bremsstrahlung distribution function of photons in the electron, we use the Weizacker-Williams distribution. Finally, $f_{\gamma/e}^{beam}(x)$, the beamstrahlung distribution function of photons inside the electron, is related to $f_{e/e}^{beam}(x)$, and is again determined by the values of Υ, σ_z and E_e [29].

As an illustration, we plot in Fig. 1 the electron bremsstrahlung distribution function (dashed curve), the electron beamstrahlung distribution (dot-dashed curve) and the convolution (solid curve). For the beamstrahlung function, we take $E_e = 250$ GeV, $\Upsilon = 0.1072$, and $\sigma_z = 0.12$ mm, typical for a $\sqrt{s} = 500$ GeV e^+e^- LC using X-band klystron accelerating technology. We see that the distribution of electrons within the electron is strongly peaked at $x \simeq 1$, and that there is a long tail extending to low fractional momentum x.

In Fig. 2, we show the corresponding bremsstrahlung (solid) and beamstrahlung (dashed) distribution functions for photons inside the electron, for the same beam parameters as in Fig. 1. In this case, both distribution functions are sharply peaked at $x \sim 0$, which indicates the presence of an intense cloud of soft photons accompanying the beam of electrons in a linear collider. The bremsstrahlung photon distribution function remains significant out to large $x \sim 1$, while the beamstrahlung photon distribution function (which is anti-correlated with the corresponding electron distribution) completely dies off for large x.

The tree level subprocess cross section for $e^+e^- \to f\bar{f}$ via s-channel γ and Z exchange can be found in many texts (see for instance Ref. [30]). The $\gamma\gamma \to f\bar{f}$ subprocess cross section can be easily constructed by crossing, along with appropriate replacements of electric charge and color factors from the $e^+e^- \to \gamma\gamma$ cross section given, for instance, in Ref. [31]. In Fig. 3, we show the distribution of tau pair invariant mass for $e^+e^- \to \tau^+\tau^-$ events at a $\sqrt{s} = 500$ GeV LC, using the same beamstrahlung parameters as in Fig. 1. We have required that $p_T(\tau) > 5$ GeV and $|\eta_\tau| < 2.5$. The solid histogram represents the contribution from the $\hat{\sigma}(e^+e^- \to \tau^+\tau^-)$ cross section. The peak at $m(\tau^+\tau^-) = 500$ GeV originates in the peak of the electron PDF $f_{e/e}(x,Q^2)$ at $x = 1$. In addition, the peak from the radiative return to the Z resonance is clearly visible at at $m(\tau^+\tau^-) = M_Z$. We note that the enhancement that would be expected to occur at $x \sim 0$ due to the photon exchange in

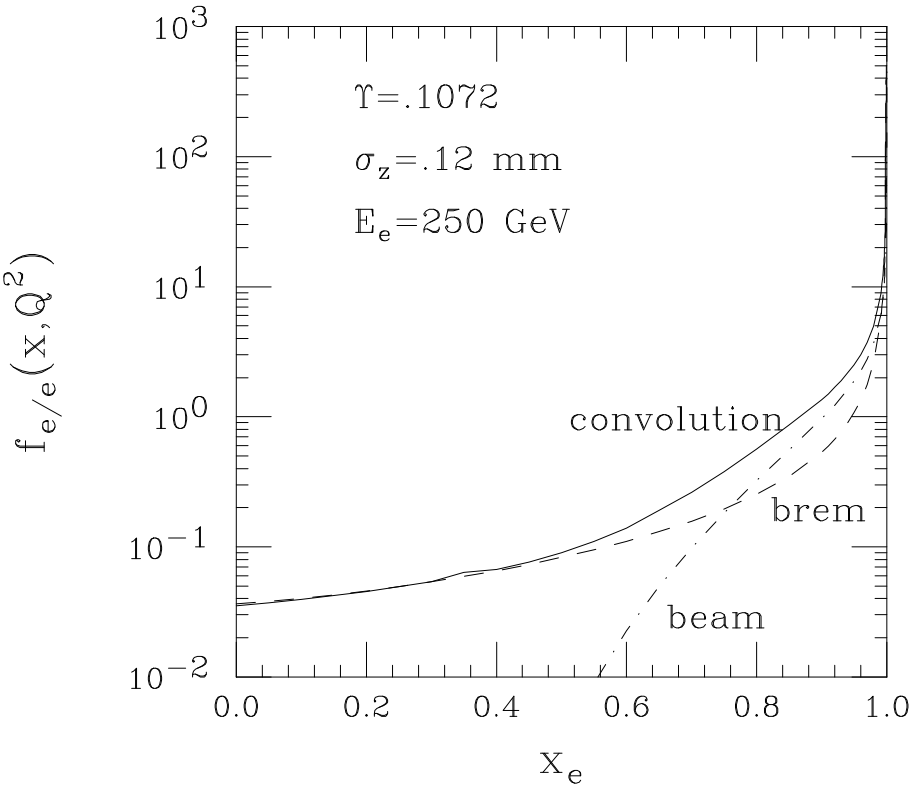

Figure 1: Electron parton distribution functions in the electron from bremsstrahlung and from beamstrahlung, along with their convolution, for $E_{beam} = 250$ GeV, $\Upsilon = 0.1072$ and $\sigma_z = 0.12$ mm.

the subprocess amplitude is eliminated by the p_T and $|\eta|$ cuts. We also plot as the dashed histogram the contribution to tau pair production from the $\gamma\gamma \to \tau^+\tau^-$ subprocess cross section. It can be seen that this contribution completely dominates the tau pair production cross section for invariant masses below about $\sqrt{\hat{s}} \sim 250$ GeV. In particular, it completely overwhelms the Z resonance peak, and has the potential to yield a formidable background for signal events with only relatively soft fermions as visible particles in the final state.

The various $\gamma\gamma \to f\bar{f}$ subprocess cross sections for SM fermions have been incorporated into the event generator Isajet v7.70[26], along with the photon bremsstrahlung and beamstrahlung distribution functions. Electron bremsstrahlung and beamstrahlung distributions had already been incorporated previously.

3. Reach for SUSY in the stau co-annihilation region

Our goal in this section is to evaluate the reach of an e^+e^- LC for SUSY in the stau co-annihilation region by searching for stau pair production events. Most earlier studies have identified the reach of a LC for SUSY in the stau co-annihilation region by searching for e^+e^- or $\mu^+\mu^-$ pairs which would originate from selectron or smuon pair production[32, 33, 23]; see, however, Ref. [34] for a study of stau signals at the LC. In the mSUGRA model at low values of $\tan\beta$, the $\tilde{\tau}_1$, $\tilde{e}_1$ and $\tilde{\mu}_1$ all tend to be nearly degenerate in mass. As $\tan\beta$ increases, the τ Yukawa coupling increases, which helps to drive the $\tilde{\tau}_L$ and $\tilde{\tau}_R$ soft

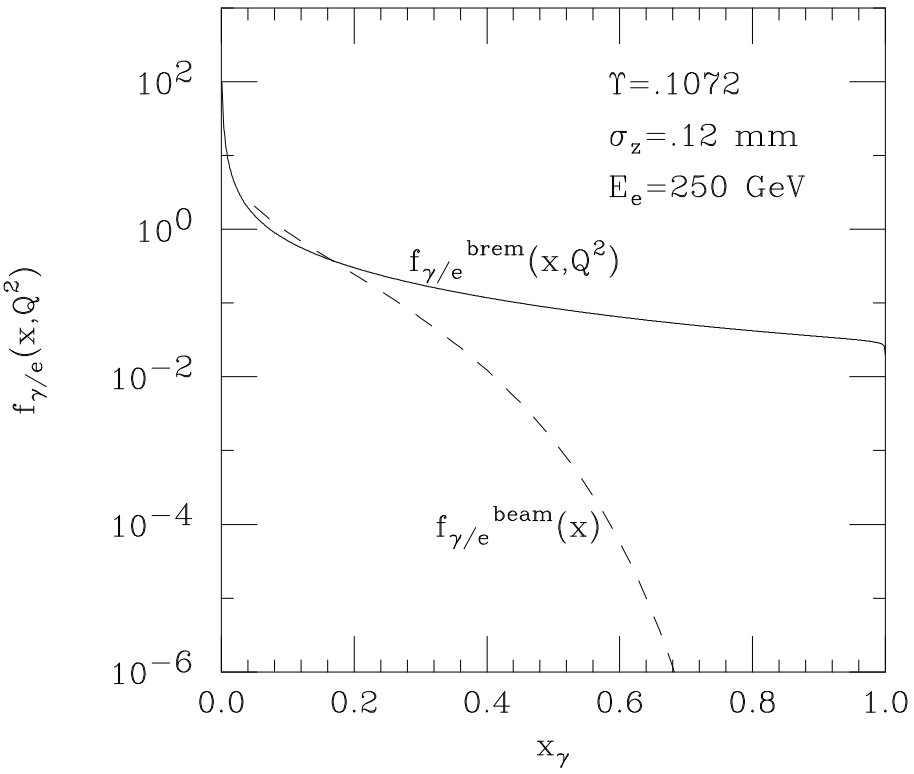

Figure 2: Photon parton distribution functions in the electron from bremsstrahlung and from beamstrahlung, for $E_{beam} = 250$ GeV, $\Upsilon = 0.1072$ and $\sigma_z = 0.12$ mm.

SUSY breaking masses to values lower than their first and second generation counterparts. In addition, if $\tan\beta$ is large, mixing between $\tilde{\tau}_L$ and $\tilde{\tau}_R$ states reduces $m_{\tilde{\tau}_1}$ even further. Thus, for low m_0 and large $\tan\beta$, it turns out that $m_{\tilde{\tau}_1}$ can be significantly lighter than the lightest selectrons or smuons. In this case, there should exist portions of mSUGRA model parameter space where $\sigma(e^+e^- \to \tilde{\tau}_1^+\tilde{\tau}_1^-)$ is large, while $\sigma(e^+e^- \to \tilde{e}_1^+\tilde{e}_1^-)$ and $\sigma(e^+e^- \to \tilde{\mu}_1^+\tilde{\mu}_1^-)$ are kinematically suppressed or forbidden.

For all our computations, we use Isajet 7.70[26] which allows for the use of polarized beams, and also allows for convolution of subprocess cross sections with electron and photon PDFs to incorporate initial state bremsstrahlung as well as beamstrahlung effects. We use the Isajet toy detector CALSIM with calorimetry covering the regions $-4 < \eta < 4$ with cell size $\Delta\eta \times \Delta\phi = 0.05 \times 0.05$. Electromagnetic energy resolution is given by $\Delta E_{em}/E_{em} = 0.15/\sqrt{E_{em}} \oplus 0.01$, while hadronic resolution is given by $\Delta E_h/E_h = 0.5/\sqrt{E_h} \oplus 0.02$, where $\oplus$ denotes addition in quadrature, and energy is measured in GeV. Jets are identified using the Isajet jet finding algorithm GETJET using a fixed cone size of $\Delta R = \sqrt{\Delta\eta^2 + \Delta\phi^2} = 0.6$, modified to cluster on energy rather than transverse energy. Clusters with $E > 5$ GeV and $|\eta(jet)| < 2.5$ are labeled as jets. Muons and electrons are classified as isolated if they have $E > 5$ GeV, $|\eta_\ell| < 2.5$, and the visible activity within a cone of $R = 0.5$ about the lepton direction is less than $max(E_\ell/10 \text{ GeV}, 1 \text{ GeV})$. Finally, "$\tau$-jets" are defined as jets fulfilling the above jet criteria, but in addition having just one or three charged tracks

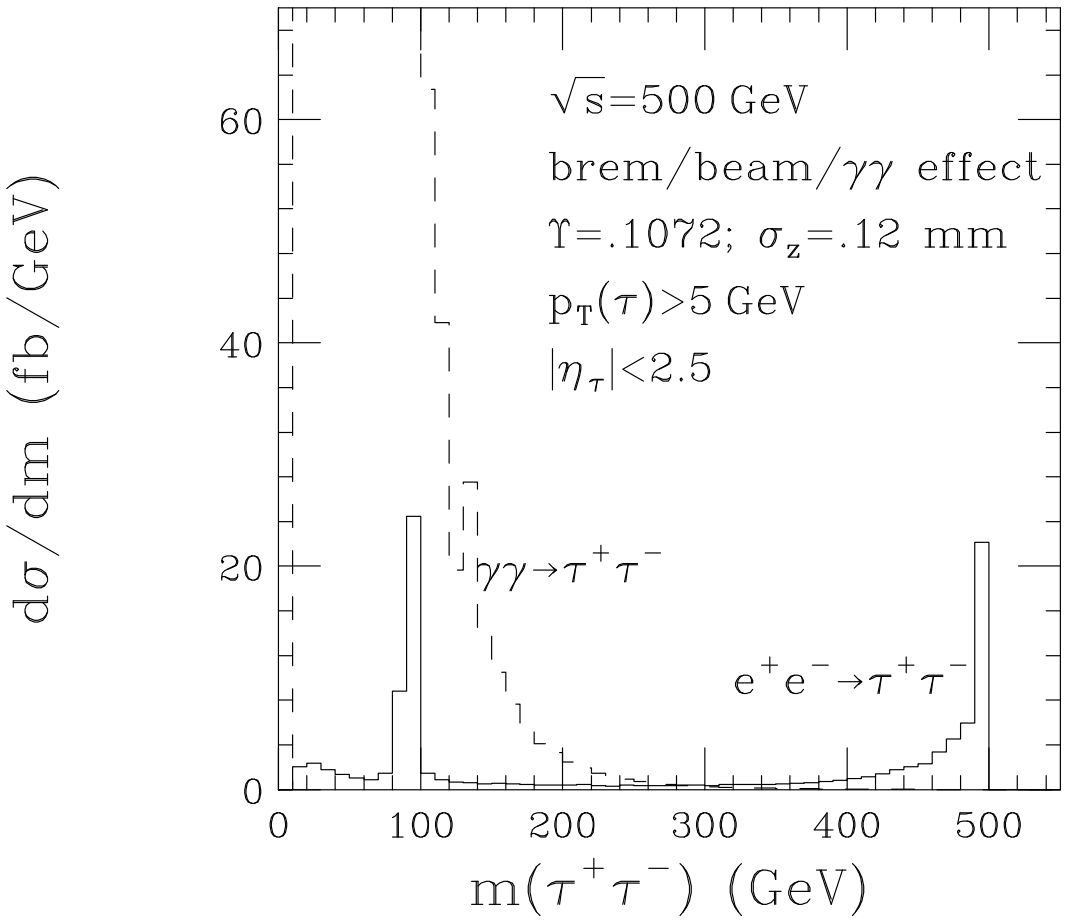

Figure 3: Distribution in di-tau invariant mass from $e^+e^- \to \tau^+\tau^-$ at a $\sqrt{s} = 500$ GeV linear e^+e^- collider including bremsstrahlung and beamstrahlung effects, and the two-photon annihilation contribution, for $E_{beam} = 250$ GeV, $\Upsilon = 0.1072$ and $\sigma_z = 0.12$ mm. Cuts described in the text have been implemented.

included within the jet cone.[2]

In this section, we assume an integrated luminosity of 100 fb^{-1} for both a $\sqrt{s} = 500$ and 1000 GeV e^+e^- LC. We assume right polarized electron beams with $P_L(e^-) = -0.9$, to minimize SM background from W pair production, with no cost and even a modest enhancement of the stau signal.

We generate SUSY signal events in the mSUGRA model parameter space, plus all $2 \to 2$ SM background processes as incorporated into Isajet. We then require both signal and background events with

- no isolated leptons,
- two tau jets.

[2]This tends to overestimate the chance that a QCD jet fakes a tau jet. We will see, however, that our cuts are efficient in removing this non-physics background, and the reach in channels involving tau is ultimately limited by the SM sources of taus.

The requirement of two jets restricts $E_{vis} > 10$ GeV, as each jet has $E > 5$ GeV. At this point, the signal in the stau co-annihilation region is dominated by tau jet pairs originating from stau pair production, while background is dominated by $\gamma\gamma \to \tau^+\tau^-$ production. The background $\tau^+\tau^-$ pair comes out back-to-back in the transverse plane, and this correlation is largely maintained by the visible tau jets. The distribution in $\cos\phi(jj)$, the dijet opening angle in the transverse plane, is shown in the first frame of Fig. 4 for the $\tau^+\tau^-$ background (red histogram) and all other SM backgrounds (*e.g.* WW, ZZ production, *etc.*) (black histogram). The signal distribution is shown in the upper right frame, for the mSUGRA point $m_0 = 200$ GeV, $m_{1/2} = 520$ GeV, $A_0 = 0$, $\tan\beta = 30$ and $\mu > 0$. We also take $m_t = 180$ GeV. While the signal has some peak near $\cos\phi(jj) \sim -1$, it maintains a broad distribution for all other $\cos\phi(jj)$ values. The $\gamma\gamma \to \tau^+\tau^-$ background is, however, much more sharply peaked at $\cos\phi(jj) \sim -1$, which leads us to propose the cut:

- $\cos\phi(jj) > -0.9$.

After the $\cos\phi(jj)$ cut, we show the distributions for background and signal events in missing transverse energy $\not{E}_T$ (middle two frames) and visible energy $E_{visible}$ (lower two frames). The optimal cuts in these latter two quantities vary depending on where one is in parameter space. We examine the possibilities:

- $\not{E}_T > 0,\ 5,\ 10, \cdots,\ 195,\ 200$ GeV, and
- $E_{visible} < 15,\ 20,\ 25,\ \cdots,\ 495,\ 500$ GeV.

For each set of possibilities, we consider only cases with at least 10 signal events for 100 fb^{-1} of integrated luminosity. We then pick the set of $\not{E}_T$, $E_{visible}$ cuts which maximizes the $S/(S+B)$ ratio (S = signal and B = background) and at the same time yields a 5σ signal which is our criterion for observability against SM backgrounds.[3] For the parameter space point shown in Fig. 4, the total cross section before cuts is $\sigma(e^+e^- \to \tilde{\tau}_1^+\tilde{\tau}_1^-) = 17.65$ fb. The optimal cuts turn out to be $\not{E}_T > 5$ GeV and 10 GeV $< E_{visible} < 20$ GeV. Using these cuts, the signal cross section is 0.96 fb, while the background level is 2.13 fb. We have checked that $S/B \sim 0.3 - 1$ are typical.

In Fig. 5, we show the m_0 *vs.* $m_{1/2}$ mSUGRA model parameter plane for $A_0 = 0$, $\tan\beta = 30$ and $\mu > 0$. The red shaded regions are excluded either because the $\tilde{\tau}_1$ becomes the LSP (in violation of bounds from searches for stable charged relics from the Big Bang) or due to lack of REWSB. The yellow shaded region is excluded by LEP2 searches for chargino pair production, and the region below the yellow contour is excluded by LEP2 searches for a SM-like Higgs boson, assuming that this bound applies to h. We evaluate the neutralino relic density using the DarkSUSY program[35] interfaced to Isasugra. Most of

[3]We recognize that by trying many sets of cuts to optimize the signal as a function of parameters, we should include a trials factor when assessing the statistical significance of the signal. We have not done so. We remark, however, that current projections for the expected integrated luminosity of a LC are several hundred fb^{-1}. Any signal identified by cuts optimized using the first 100 fb^{-1} of integrated luminosity, should therefore be visible in subsequent runs where the analysis is performed with these same cuts so that there is no trials factor for this new analysis.

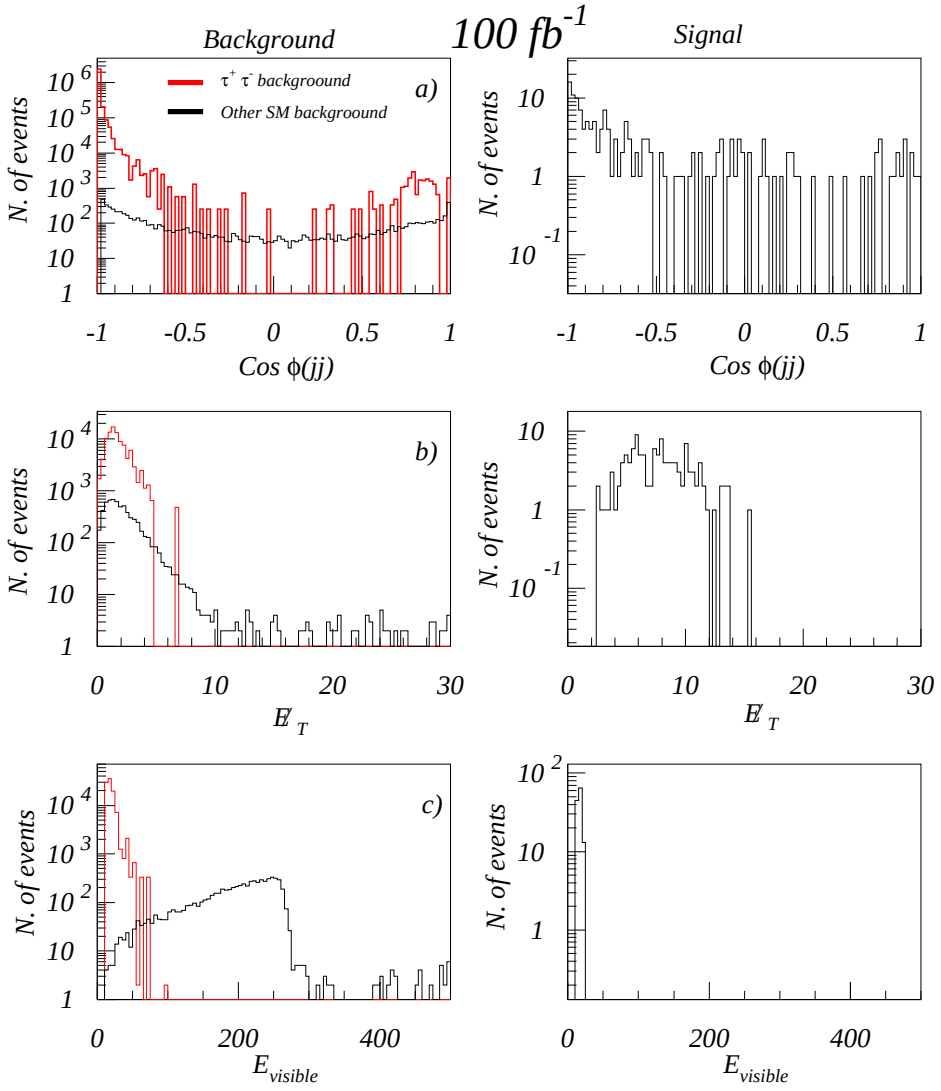

Figure 4: Distribution of events in $\cos\phi(jj)$, $\not\!\!E_T$ and $E_{visible}$ for di-tau jet+ $\not\!\!E$ events from $\tau\bar{\tau}$ production via both e^+e^- and $\gamma\gamma$ annihilation, along with background from all other SM processes (left-hand side). We also show distributions from stau pair production signal events at mSUGRA point m_0, $m_{1/2}$, A_0, $\tan\beta$, $sign(\mu) = 200$ GeV, 520 GeV, 0, 30, +1, with $m_t = 180$ GeV for a $\sqrt{s} = 500$ GeV LC (right-hand side). The relic density for this point is $\Omega_{\widetilde{Z}_1}h^2 = 0.09$.

the remaining parameter space is excluded by the WMAP bound on $\Omega_{\widetilde{Z}_1}h^2$. The exceptions occur in the blue shaded region, where $0.095 < \Omega_{\widetilde{Z}_1}h^2 < 0.129$, and where neutralinos can make up *all* the CDM of the universe, or in the green shaded region, where $\Omega_{\widetilde{Z}_1}h^2 < 0.095$, and additional CDM candidate(s) must exist to saturate the WMAP value of $\Omega_{CDM}h^2$. The thin region at low m_0 along the boundary of the excluded region is the stau co-annihilation corridor. The region at low m_0 and low $m_{1/2}$ is the bulk annihilation region, and generally gives rise to a Higgs boson mass in conflict with bounds from LEP2 searches. There is a remaining green region at low $m_{1/2}$ at the edge of the LEP2 excluded region where

neutralinos can efficiently annihilate through the light Higgs pole: $2m_{\tilde{Z}_1} \simeq m_h$. Not shown is the HB/FP region at very large m_0, since we want to focus on the stau co-annihilation region in this section.

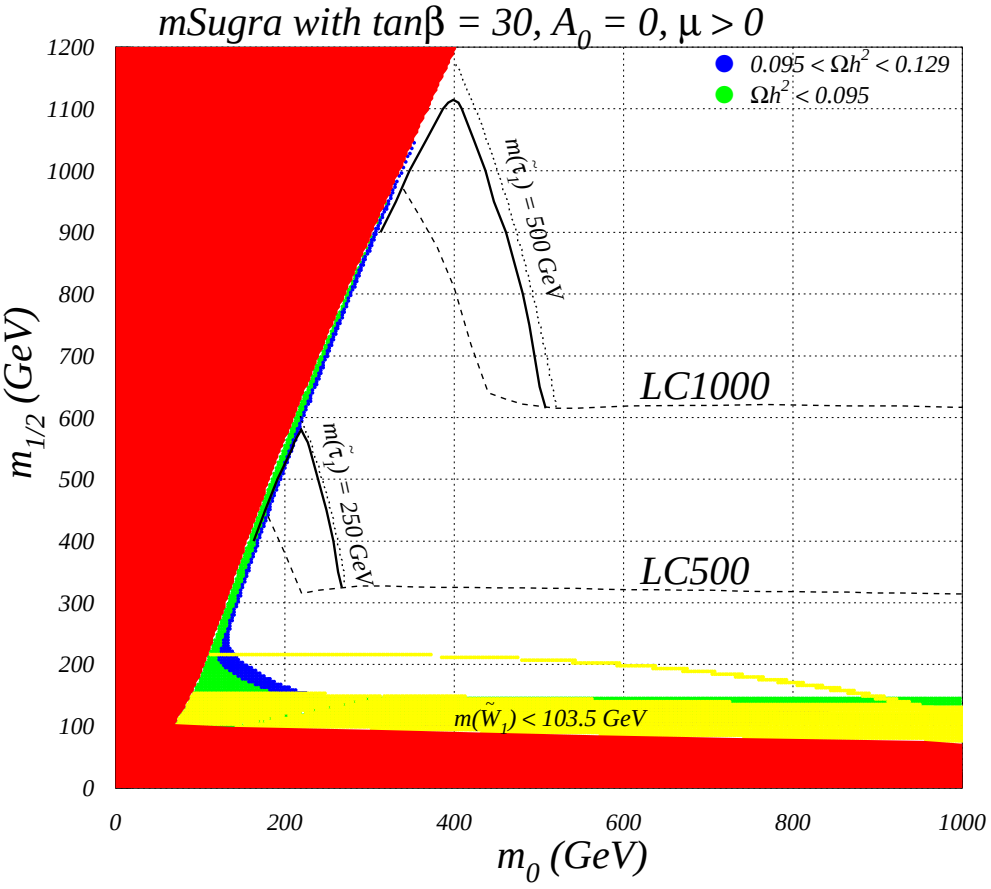

Figure 5: Reach of a linear collider for supersymmetry in the mSUGRA model for $\sqrt{s} = 500$ and 1000 GeV in the stau co-annihilation region, for $\tan\beta = 30$, $A_0 = 0$ and $\mu > 0$. The reach via selectron, smuon and chargino pair searches is denoted by the dashed contours, while the additional reach due to stau pair production is denoted by the solid contour. The dotted contour denotes the kinematic limit for stau pair production. The red region is theoretically excluded, while the yellow region is excluded by LEP2 measurements. Below the yellow contour, $m_h \leq 114.4$ GeV. The blue region is within the WMAP $\Omega_{\tilde{Z}_1}h^2$ 2σ limit, while the green region has $\Omega_{\tilde{Z}_1}h^2$ below the WMAP 2σ limit.

The dashed contours in Fig. 5 denote the reach of a $\sqrt{s} = 500$ GeV or 1000 GeV e^+e^- LC for SUSY as calculated in Ref. [23]. For the $\sqrt{s} = 1000$ GeV runs, we use $\Upsilon = 0.29$ and $\sigma_z = 0.11$ mm. The horizontal portion of the contour denotes the upper limit of parameter space which is explorable via chargino pair searches, while the rising dashed contour at lower m_0 values gives the reach in mSUGRA due to selectron and smuon searches. The dotted contours denote the kinematic limit for stau pair production at a 500 or 1000 GeV LC. The solid contour marks the boundary of the added region where there is a 5σ signal for di-tau jet events, assuming 100 fb^{-1} of integrated luminosity. From these contours, we

see that a linear e^+e^- collider can see most of the additional parameter space which is accessible to stau pair searches. However, when $m_{\tilde{\tau}_1} \simeq m_{\widetilde{Z}_1}$ along the border of parameter space, the tiny mass gap $m_{\tilde{\tau}_1} - m_{\widetilde{Z}_1}$ yields very low visible energy, and the search contours turn over. Thus, in the $\tan\beta = 30$ case shown, a direct search for stau pair production allows only a portion of the WMAP allowed region to be covered. We note here that we have also investigated stau pair signals consisting of an isolated lepton plus a single tau jet. In this case, no additional reach was obtained, and in some cases the reach is even diminished, due to the large backgrounds (mainly from WW events) in the $\ell + \tau$-jet channel. We also note here that we have investigated the lower $\tan\beta = 10$ value. In this case, $m_{\tilde{\tau}_1} \simeq m_{\tilde{e}_R}$, and hardly any reach is gained by looking for SUSY in the tau pair channel, as opposed to the dielectron or dimuon channels.

In Fig. 6, we show the same m_0 *vs.* $m_{1/2}$ plane, except we now take $\tan\beta = 45$ and $\mu < 0$. The shaded regions and contours denote the same constraints as in Fig. 5. The most noteworthy point is that the WMAP allowed region has greatly expanded compared to the $\tan\beta = 30$, $\mu > 0$ case shown in Fig. 5. This is because the A annihilation funnel has moved into the parameter space shown, and overlaps with the stau co-annihilation region. We can also see that in this case, the additional reach gained by the ditau-jet signal is considerable, and covers a rather large swath of the WMAP allowed region, for both a 500 GeV LC as well as for a 1000 GeV LC.

In Fig. 7, we again show the mSUGRA model m_0 *vs.* $m_{1/2}$ plane, but now for $\tan\beta = 52$ and $\mu > 0$. In this case, the excluded region where $\tilde{\tau}_1$ is the LSP has greatly expanded, owing to the large τ Yukawa coupling and large left-right mixing, both of which act to reduce the $\tilde{\tau}_1$ mass relative to $m_{\tilde{e}_R}$ and $m_{\tilde{\mu}_R}$. In this plot, the A annihilation funnel is not apparent (it would be located in the low m_0 excluded region) , but its effect is felt over much of the parameter space by adding to (via off-shell A and H annihilations) the stau annihilation and bulk annihilation cross sections, and thus enlarging these regions. We can see that in this case, the additional reach gained by the stau-pair search allows a $\sqrt{s} = 500$ GeV e^+e^- collider to fully access the bulk annihilation region at low m_0 and low $m_{1/2}$, which would otherwise not be accessible to searches for first and second generation sleptons. In addition, some portion of the stau co-annihilation region can also be explored by the di-tau signal, although the region with nearly degenerate $\tilde{\tau}_1$ and $\widetilde{Z}_1$ remains inaccessible due to the tiny mass gap, and low visible energy release from tau slepton decays. Likewise, the $\sqrt{s} = 1000$ GeV LC can explore all this and more, including a substantial chunk of the stau co-annihilation corridor, provided the mass gap between $\tilde{\tau}_1$ and $\widetilde{Z}_1$ is large enough to yield a sufficient rate for observable signals after cuts.

We note in passing that in the stau coannihilation region the reach of the LHC exceeds that of even the 1 TeV LC [23].

4. Reach in the HB/FP region for $m_t = 180$ GeV

In Ref. [23], chargino pair production was examined against SM backgrounds using a set of standard cuts first suggested in Ref. [32]. Briefly, the standard chargino pair cuts are as follows. Following Refs. [32] and [33], it was required to have one isolated lepton plus two

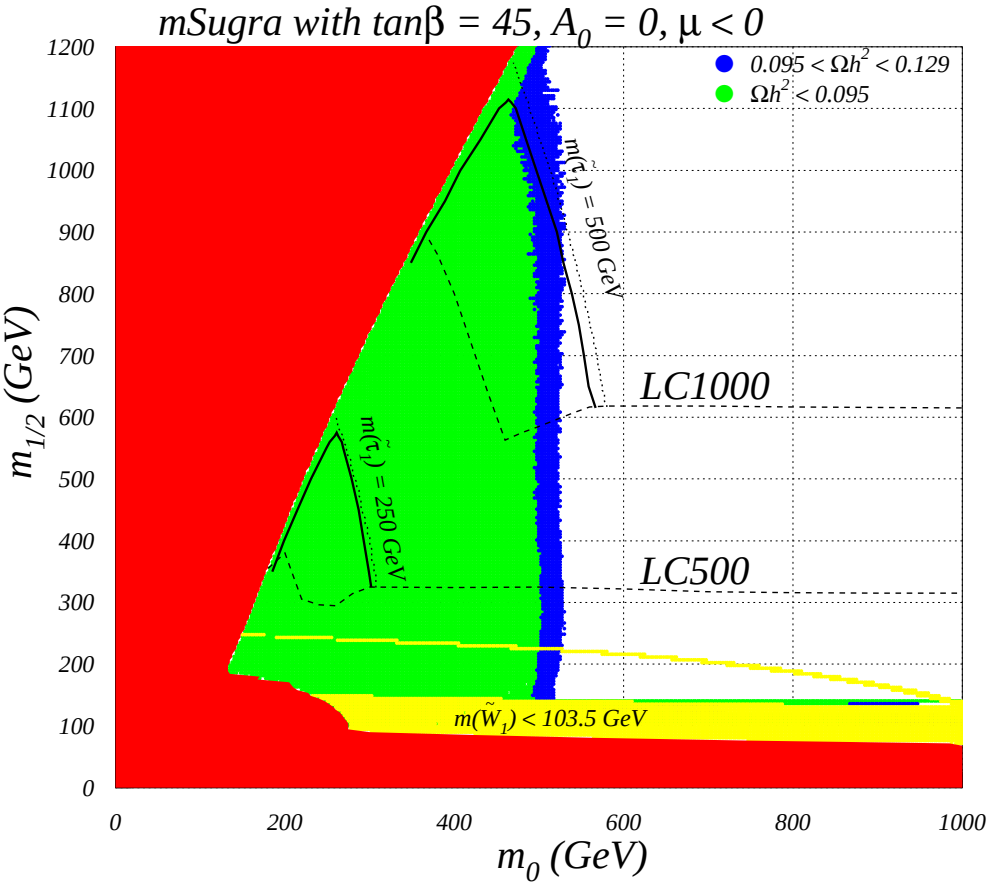

Figure 6: Reach of a linear collider for supersymmetry in the mSUGRA model for $\sqrt{s} = 500$ and 1000 GeV in the stau co-annihilation region, for $\tan\beta = 45$, $A_0 = 0$ and $\mu < 0$. The contours and shadings are as in Fig. 5.

jets with, *i*) 20 GeV $< E_{vis} < \sqrt{s} - 100$ GeV, *ii*) if $E_{jj} > 200$ GeV, then $m(jj) < 68$ GeV, *iii*) $E_T^{mis} > 25$ GeV, *iv*) $|m(\ell\nu) - M_W| > 10$ GeV for a W pair hypothesis, *v*) $|\cos\theta(j)| < 0.9$, $|\cos\theta(\ell)| < 0.9$, $-Q_\ell \cos\theta_\ell < 0.75$ and $Q_\ell \cos\theta(jj) < 0.75$, *vi*) $\theta_{acop}(WW) > 30^\circ$, for a W pair hypothesis. The reach for $1\ell + 2j + \not{E}_T$ events from chargino pair production was evaluated using a left polarized beam with $P_L = +0.9$. These cuts worked well for almost all of parameter space, save for the large $m_{1/2}$ portion of the HB/FP region. In that region, the $\widetilde{W}_1 - \widetilde{Z}_1$ mass gap becomes so small that there is very little energy release in chargino pair production events, and the signal would usually fail the standard cuts. A specialized set of cuts was proposed in Ref. [23] to access the signal in the large $m_{1/2}$ portion of the HB/FP region. These require:

- 1 isolated lepton plus two jets,
- 20 GeV$< E_{visible} <$ 100 GeV,
- $\cos\phi(jj) > -0.6$,
- $m(\ell, j_{near}) > 5$ GeV.

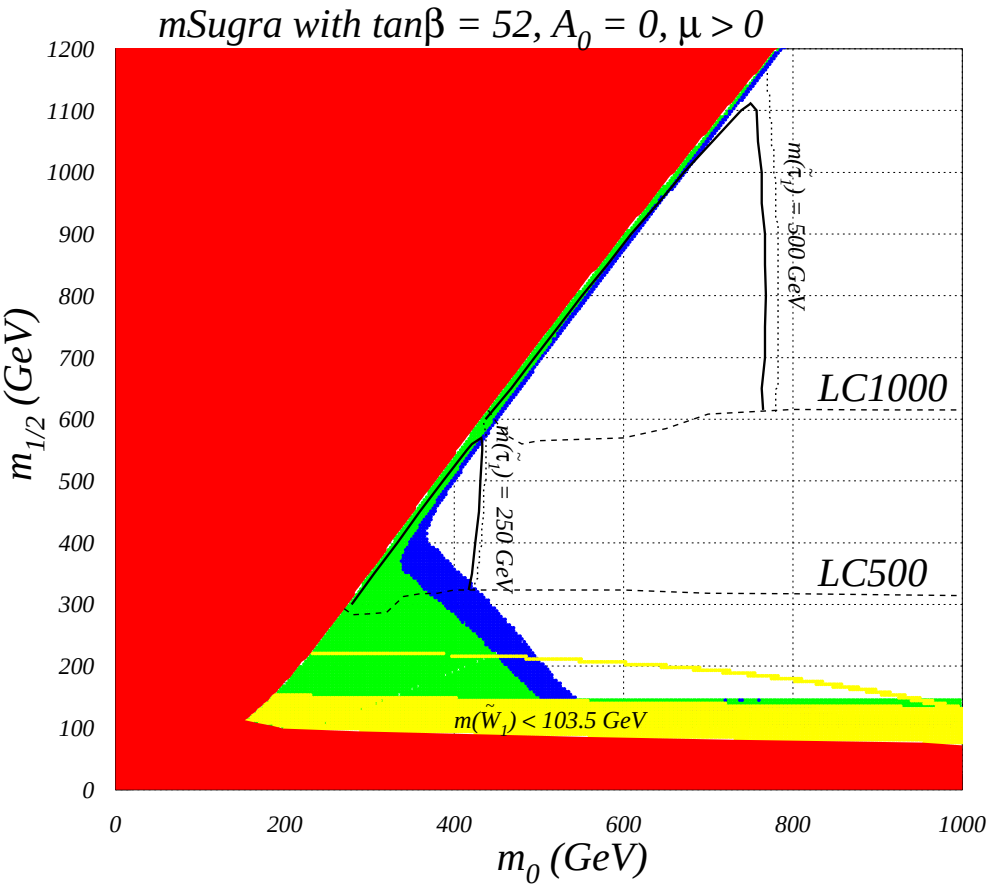

Figure 7: Reach of a linear collider for supersymmetry in the mSUGRA model for $\sqrt{s} = 500$ and 1000 GeV in the stau co-annihilation region, for $\tan\beta = 52$, $A_0 = 0$ and $\mu > 0$. The contours and shadings are as in Fig. 5.

The cut on $\cos\phi(jj)$ is on the dijet opening angle in the transverse plane. Backgrounds from $2 \to 2$ processes were evaluated with Isajet, while $\gamma\gamma \to f\bar{f}$ background was evaluated using Pythia, which included only the bremsstrahlung portion of the photon PDF. The total SM background from $2 \to 2$ processes plus $\gamma\gamma \to f\bar{f}$ was found to be 0.97 fb for a $\sqrt{s} = 500$ GeV LC. Using these cuts, it was found that the chargino pair signal could be seen essentially up to the kinematic limit even in the high $m_{1/2}$ portion of the HB/FP region where there is no observable signal at the LHC.

In this section, we re-examine the chargino pair signal, but this time including as well the $\gamma\gamma \to c\bar{c}$ and $b\bar{b}$ backgrounds from both bremsstrahlung and beamstrahlung, as incorporated into Isajet 7.70. The background estimate from $2 \to 2$ processes plus $\gamma\gamma \to f\bar{f}$ obtained for a $\sqrt{s} = 500$ GeV LC with $\Upsilon = 0.1072$ and $\sigma_z = 0.12$ mm is now 44.1 fb, after the above cuts are applied - an increase by a factor of ~ 40! (The background level using standard cuts hardly changes after including beamstrahlung photons, since that set of cuts is also adept at removing the $\gamma\gamma$ background.)

The situation is illustrated in Fig. 8, where we show the distribution in $\cos\theta(j)$ for the

most energetic jet in signal and background events which pass the specialized HB/FP cuts. The mSUGRA model signal point is taken to be $m_0 = 8850$ GeV, $m_{1/2} = 400$ GeV, $A_0 = 0$, $\tan\beta = 30$ and $\mu > 0$, where we have adopted the value $m_t = 180$ GeV for the top quark mass. It is seen from Fig. 8 that the signal events have a broad distribution in $\cos\theta(j)$, while the background distribution is sharply peaked at $|\cos\theta(j)| \sim 1$. Considerable suppression of the $\gamma\gamma \to c\bar{c},\ b\bar{b}$ background at little cost to signal can thus be gained by requiring in addition

- $|\cos\theta(j)| < 0.8$,

which we apply to both jets in the $\ell + 2 - jet$ events. After applying this cut, the $2 \to 2$ plus $\gamma\gamma$ background level drops from 44.1 fb to 0.39 fb. The signal cross section for the parameter space point shown drops from 39.5 fb to 28.8 fb. We have re-evaluated the reach projections in the m_0 *vs.* $m_{1/2}$ plane of Ref. [23] after including the updated background including beamstrahlung and the additional $|\cos\theta(j)|$ cut, and find that the reach projections suffer no visible change.

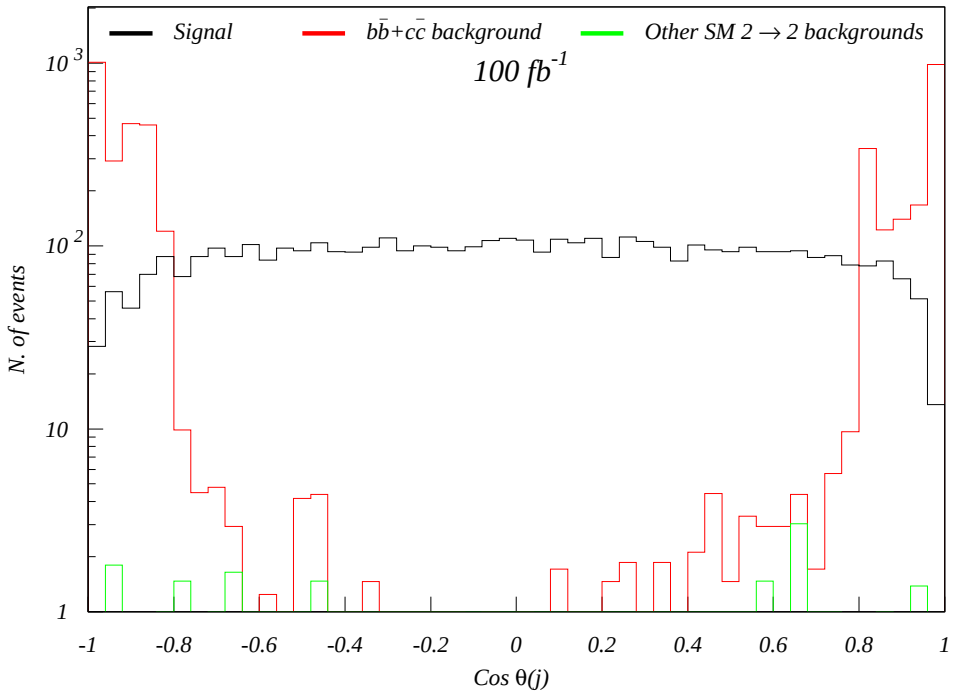

Figure 8: The angular distribution of the hardest jet in $\ell + jj + \not{E}$ events from sparticle pair production at mSUGRA point m_0, $m_{1/2}$, A_0, $\tan\beta$, $sign(\mu)$ = 8850, 400, 0, 30, +1, with $m_t = 180$ GeV for a $\sqrt{s} = 500$ GeV LC. The relic density for this point is $\Omega_{\widetilde{Z}_1} h^2 = 0.09$. We show background from $b\bar{b}$ and $c\bar{c}$ production via both e^+e^- and $\gamma\gamma$ annihilation, along with background from all other SM processes.

After the publication of Ref. [23], the DØ Collaboration has announced a re-analysis of old data on top quark pair production, using more sophisticated techniques that retain

more information about the event shapes for extracting the top quark mass in the $\ell + jets$ channel[8]. They now find a value $m_t = 180.1 \pm 5.3$ GeV, which has smaller error bars and a significantly larger value of m_t than previous measurements. Combined with CDF measurements, the two experiments find a world average $m_t = 178.0 \pm 4.3$ GeV[36]. The value of m_t is an important parameter in determining the location of the HB/FP region in the mSUGRA model[18]. We take this opportunity to update our mSUGRA reach projections assuming a value of $m_t = 180$ GeV, whereas previous results used $m_t = 175$ GeV[23].

To illustrate the effect of the higher top quark mass, we show in Fig. 9 the m_0 *vs.* $m_{1/2}$ plane for $A_0 = 0$, $\tan\beta = 30$ and $\mu > 0$. The main effect of the increased value of m_t is to push the HB/FP region from the vicinity of $m_0 \sim 3 - 8$ TeV (for $m_t = 175$ GeV) to $m_0 \sim 8 - 14$ TeV (for $m_t = 180$ GeV). Another less noticable effect is that the larger m_t value increases the relative value of m_h via radiative corrections, so that the region of good relic density from neutralino annihilation via s-channel h exchange has been pulled to larger $m_{1/2}$ values. This light higgs annihilation corridor is shown as a discontinuous narrow band around $m_{1/2} \sim 150$ GeV in the figure.

We also show the reach of the Tevatron via the isolated trilepton channel (following procedures listed in Ref. [18]), and the reach of the CERN LHC (following procedures listed in Ref. [22]). The LC reach is plotted as in Ref. [23]. The Tevatron reach contour here is plotted assuming a 5σ signal with 10 fb^{-1} of integrated luminosity. It remains qualitatively similar to the $\tan\beta = 30$, $m_t = 175$ GeV case, except that it is effectively stretched out in m_0. The light Higgs annihilation corridor, which was not apparent for $\tan\beta = 30$, $m_t = 175$ GeV, is now visible, and within the reach of the Fermilab Tevatron. The LHC reach contour, plotted for a 5σ signal with 100 fb^{-1} of integrated luminosity, extends to $m_{1/2} \sim 1300$ GeV for low m_0 (corresponding to a value of $m_{\tilde{g}} \sim 3$ TeV). As m_0 increases, the contour drops until $m_0 \sim 3$ TeV is reached, whereupon it levels out and stays roughly constant in $m_{1/2} \sim 700$ GeV (corresponding to a value $m_{\tilde{g}} \sim 1.8$ TeV). What is happening is that as m_0 increases, squarks become increasingly heavy, while $m_{\tilde{g}}$ remains roughly constant for a given value of $m_{1/2}$. Thus, at $m_0 \sim 3$ TeV, the squark contribution to LHC signals has essentially decoupled, and almost all the SUSY signal originates from gluino pair production, followed by gluino cascade decays. The LC reach plots are qualitatively similar to those presented in Ref. [23], except that they are stretched out in m_0 until the HB/FP region is reached. As expected, this reach is mainly governed by the chargino mass and the mass gap between the chargino and the LSP. We note here that the shift in the HB/FP region to very large values of m_0 for $m_t = 180$ GeV can be viewed favorably for SUSY theories, in that the large scalar masses will give further suppression to possible flavor changing or CP violating processes[37, 13].

5. Conclusions

Significant portions of the mSUGRA parameter space where the neutralino relic density is in accord with WMAP analyses occur around the boundaries of parameter space in the mSUGRA region. These boundaries occur where $m_{\tilde{\tau}_1} - m_{\tilde{Z}_1} \to 0$ in the stau co-

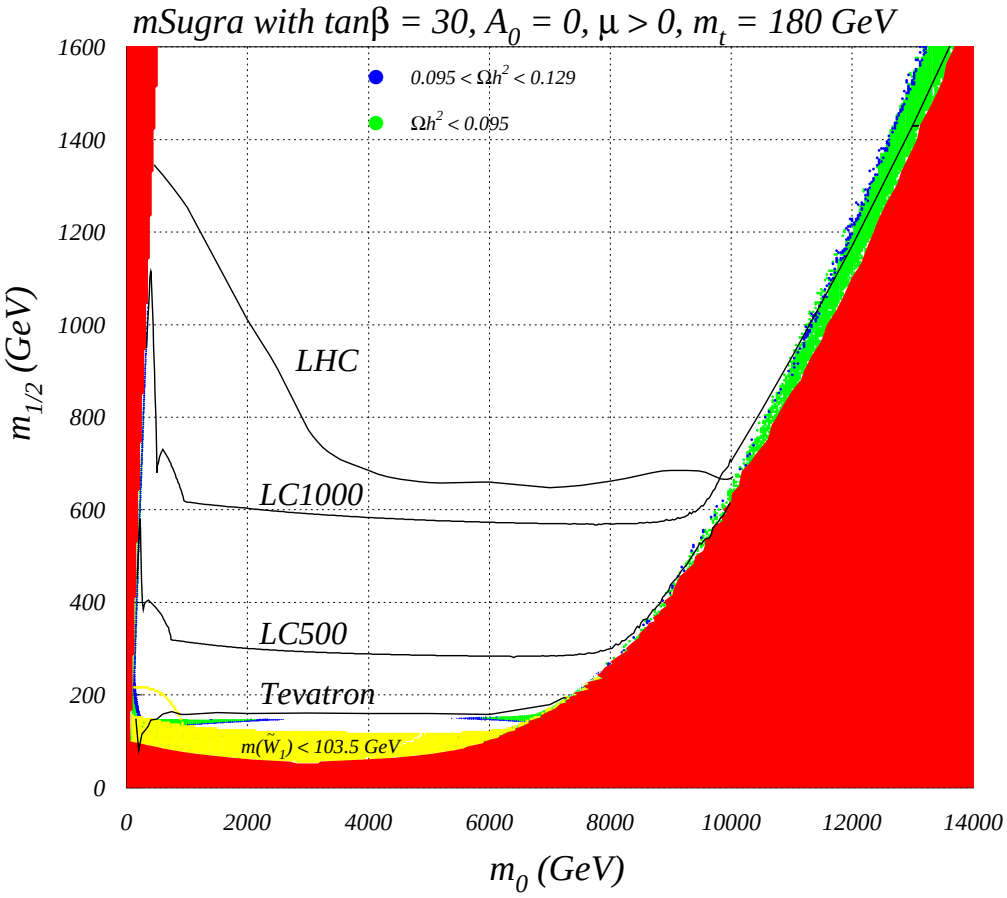

Figure 9: Reach of the Fermilab Tevatron, CERN LHC and a linear collider for supersymmetry in the mSUGRA model for $\sqrt{s} = 500$ and 1000 GeV for $\tan\beta = 30$, $A_0 = 0$, $\mu > 0$ and $m_t = 180$ GeV. The red region is theoretically excluded, while the yellow region is excluded by LEP2 measurements. Below the yellow contour, $m_h \leq 114.4$ GeV. The blue region is within the WMAP $\Omega_{\tilde{Z}_1} h^2$ 2σ limit, while the green region has $\Omega_{\tilde{Z}_1} h^2$ below the WMAP 2σ limit.

annihilation region or where $m_{\widetilde{W}_1} - m_{\tilde{Z}_1} \to 0$ in the HB/FP region. In these regions, pair production of NLSPs will result in collider events with very low energy release, and low invariant mass. The process $\gamma\gamma \to f\bar{f}$ where the γs come from initial state bremsstrahlung or beamstrahlung is also highly peaked at low $f\bar{f}$ invariant mass, and may thus constitute an important background process in these DM allowed regions of parameter space.

We have incorporated $\gamma\gamma \to f\bar{f}$ into the Isajet event generator for e^+e^- collisions. This enables us to evaluate signal and background rates for $e^+e^- \to \tilde{\tau}_1^+\tilde{\tau}_1^- \to \tau\bar{\tau} + \not{E}_T$ production in the stau co-annihilation region. Using suitable cuts to tame the $\gamma\gamma \to \tau\bar{\tau}$ background, we find that significant regions of additional reach are obtained, especially if $\tan\beta$ is large.

We have also investigated the $\gamma\gamma \to c\bar{c},\ b\bar{b}$ background to $e^+e^- \to \widetilde{W}_1^+\widetilde{W}_1^- \to \ell + jj + \not{E}_T$ production in the HB/FP region of the mSUGRA model. Inclusion of the beamstrahlung backgound significantly increases the SM background for this signal. However, the addi-

tional background can be effectively removed by requiring the jets to be away from the beam directions.

We update our mSUGRA reach plots for $\tan\beta = 30$ by increasing the value of m_t from 175 GeV to 180 GeV, in accord with recent $D\emptyset$ measurements. This has the effect of pushing the HB/FP region out to much large values of m_0, and effectively stretching out the reach contours for the Fermilab Tevatron, the CERN LHC and an e^+e^- LC. Expressed in terms of the chargino mass, the reach in the HB/FP region is qualititatively unaltered.

Acknowledgments

We thank M. Drees for providing us with his subroutines which calculate beamstrahlung distributions. This research was supported in part by the U.S. Department of Energy under contract numbers DE-FG02-97ER41022 and DE-FG03-94ER40833.

References

[1] For recent reviews, see *e.g.* S. Martin, in *Perspectives on Supersymmetry*, edited by G. Kane (World Scientific), `hep-ph/9709356`; M. Drees, `hep-ph/9611409`; J. Bagger, `hep-ph/9604232`; X. Tata, *Proc. IX J. Swieca Summer School,* J. Barata, A. Malbousson and S. Novaes, Eds., `hep-ph/9706307`; S. Dawson, Proc. TASI 97, J. Bagger, Ed., `hep-ph/9712464`.

[2] H. Goldberg, *Phys. Rev. Lett.* **50** (1983) 1419; J. Ellis, J. Hagelin, D. Nanopoulos, K. Olive and M. Srednicki, *Nucl. Phys.* **B 238** (1984) 453.

[3] D. N. Spergel *et al.*, Determination of Cosmological Parameters," Ap. J. Supp. **148** (2003) 175, arXiv:astro-ph/0302209.

[4] For a review of WMAP implications for supersymmetric models, see A. Lahanas, N. E. Mavromatos and D. V. Nanopoulos, *Int. J. Mod. Phys.* **D 12** (2003) 1529.

[5] C. Alfonso *et al.* Astron. and Astrophys. **400** (2003) 951, astro-ph/0212176; C. Alcock *et al.*, Ap. J. **542** (2000) 281, astro-ph/0011506.

[6] A. Chamseddine, R. Arnowitt and P. Nath, *Phys. Rev. Lett.* **49** (1982) 970; R. Barbieri, S. Ferrara and C. Savoy, *Phys. Lett.* **B 119** (1982) 343; N. Ohta, *Prog. Theor. Phys.* **70** (1983) 542; L. J. Hall, J. Lykken and S. Weinberg, *Phys. Rev.* **D 27** (1983) 2359; for reviews, see H. P. Nilles, *Phys. Rep.* **110** (1984) 1, and P. Nath, `hep-ph/0307123`.

[7] K. Hagiwara *et al.* (Particle Data Group), *Phys. Rev.* **D 66** (2002) 010001.

[8] V. Abazov *et al.* (DØ Collaboration), Nature (2004) (in press).

[9] M. Drees and M. Nojiri, *Phys. Rev.* **D 47** (1993) 376; H. Baer and M. Brhlik, *Phys. Rev.* **D 57** (1998) 567; H. Baer, M. Brhlik, M. Diaz, J. Ferrandis, P. Mercadante, P. Quintana and X. Tata, *Phys. Rev.* **D 63** (2001) 015007; A. Djouadi, M. Drees and J. Kneur, *J. High Energy Phys.* **0108** (2001) 055; J. Ellis, T. Falk, G. Ganis, K. Olive and M. Srednicki, *Phys. Lett.* **B 510** (2001) 236; L. Roszkowski, R. Ruiz de Austri and T. Nihei, *J. High Energy Phys.* **0108** (2001) 024; A. Lahanas and V. Spanos, *Eur. Phys. J.* **C 23** (2002) 185.

[10] J. Ellis, T. Falk and K. Olive, *Phys. Lett.* **B 444** (1998) 367; J. Ellis, T. Falk, K. Olive and M. Srednicki, *Astropart. Phys.* **13** (2000) 181.

[11] J. Ellis, K. Olive, Y. Santoso and V. Spanos, *Phys. Lett.* **B 565** (2003) 176; H. Baer and C. Balázs, JCAP**0305** (2003) 006; U. Chattopadhyay, A. Corsetti and P. Nath, *Phys. Rev.* **D 68** (2003) 035005; A. Lahanas and D. V. Nanopoulos, *Phys. Lett.* **B 568** (2003) 55.

[12] K. Chan, U. Chattopadhyay and P. Nath, *Phys. Rev.* **D 58** (1998) 096004.

[13] J. Feng, K. Matchev and T. Moroi, *Phys. Rev. Lett.* **84** (2000) 2322 and *Phys. Rev.* **D 61** (2000) 075005.

[14] H. Baer, C. H. Chen, F. Paige and X. Tata, *Phys. Rev.* **D 52** (1995) 2746 and *Phys. Rev.* **D 53** (1996) 6241.

[15] See H. Baer and M. Brhlik, Ref. [9]

[16] J. Feng, K. Matchev and F. Wilczek, *Phys. Lett.* **B 482** (2000) 388 and *Phys. Rev.* **D 63** (2001) 045024.

[17] H. Baer and M. Brhlik, *Phys. Rev.* **D 53** (1996) 597.

[18] H. Baer, T. Krupovnickas and X. Tata, *J. High Energy Phys.* **0307** (2003) 020.

[19] H. Baer, C. Balazs, A. Belyaev, J. Mizukoshi, X. Tata and Y. Wang, *J. High Energy Phys.* **0207** (2002) 050 and `hep-ph/0210441`.

[20] C. Böhm, A. Djouadi and M. Drees, *Phys. Rev.* **D 30** (2000) 035012; J. Ellis, K. Olive and A. Santoso, *Astropart. Phys.* **18** (2003) 395; J. Edsjö, *et al.*, JCAP **04** (2003) 001.

[21] For earlier work on chargino detection at the luminosity upgrade of the Tevatron, see H. Baer, M. Drees, F. Paige, P. Quintana and X. Tata, *Phys. Rev.* **D 61** (2000) 095007; V. Barger and C. Kao, *Phys. Rev.* **D 60** (1999) 115015; K. Matchev and D. Pierce, *Phys. Lett.* **B 467** (1999) 225.

[22] H. Baer, C. Balazs, A. Belyaev, T. Krupovnickas and X. Tata, *J. High Energy Phys.* **0306** (2003) 054. For earlier work, see H. Baer, C. H. Chen, F. Paige and X. Tata, *Phys. Rev.* **D 52** (1995) 2746 and *Phys. Rev.* **D 53** (1996) 6241; H. Baer, C. H. Chen, M. Drees, F. Paige and X. Tata, *Phys. Rev.* **D 59** (1999) 055014; S. Abdullin and F. Charles, *Nucl. Phys.* **B 547** (1999) 60; S. Abdullin *et al.* (CMS Collaboration), `hep-ph/9806366`; B. Allanach, J. Hetherington, A. Parker and B. Webber, *J. High Energy Phys.* **08** (2000) 017.

[23] H. Baer, A. Belyaev, T. Krupovnickas and X. Tata, *J. High Energy Phys.* **0402** (2004) 007.

[24] T. Sjostrand *et al.*, *Comput. Phys. Commun.* **135** (2001) 238.

[25] M. Drees and R. Godbole, *Phys. Rev.* **D 50** (1994) 3124.

[26] H. Baer, F. Paige, S. Protopopescu and X. Tata, `hep-ph/0312045`.

[27] R. Arnowitt, B. Dutta, T. Kamon and V. Khotilovich, `hep-ph/0308159`.

[28] E. A. Kuraev and V. S. Fadin, Sov. J. Nucl. Phys. **41** (1985) 466.

[29] P. Chen, *Phys. Rev.* **D 46** (1992) 1186; see also M. Peskin, SLAC-TN-04-032.

[30] V. Barger and R. J. N. Phillips, *Collider Physics*, Perseus Press (1987).

[31] M. Peskin and D. V. Schroeder, *Introduction to Quantum Field Theory*, Westview Press (1995).

[32] T. Tsukamoto, K. Fujii, H. Murayama, M. Yamaguchi and Y. Okada, *Phys. Rev.* **D 51** (1995) 3153; see also JLC-1, KEK Report 92-16 (1992).

[33] H. Baer, R. Munroe and X. Tata, *Phys. Rev.* **D 54** (1996) 6735.

[34] M. Nojiri, K. Fujii and T. Tsukamoto, *Phys. Rev.* **D 54** (1996) 6756.

[35] DarkSUSY, P. Gondolo *et al.*, `astro-ph/0211238`, (2002).

[36] The CDF and DØ Collaborations, `hep-ex/0404010`.

[37] M. Dine, A. Kagan and S. Samuel, *Phys. Lett.* **B 243** (1990) 250.